Minimum enstrophy states and bifurcations in 2D Euler flows around a central obstacle

Florian Muller[a, @], Benoît-Joseph Gréa[b], Anne Burbeau[a], Pierre Sagaut[c]

a. CEA Saclay, DEN, DM2S/STMF, F-91191 Gif/Yvette, France
b. CEA, DAM, DIF, F-91297 Arpajon, France
c. Aix-Marseille Univ, CNRS, Centrale Marseille, M2P2 UMR 7340, 13451 Marseille, France
@ : florian.muller@cea.fr

Résumé :

Les écoulements au sein des assemblages combustibles des coeurs de réacteurs à eau pressurisée (REP) sont majoritairement alignés avec les axes des crayons. Cependant des écoulements secondaires existent dans les plans orthogonaux à ces axes et jouent un rôle essentiel dans la redistribution thermique du coeur. Ces écoulements présentent des réorganisations spontanées qui semblent comparables aux changements de phase observés entre des états méta-stables de l'atmosphère de l'hémisphère Nord (~~Corvellec~~ [5]). Pour avancer une explication de ce phénomène, nous calculons des états d'équilibre des équations d'Euler en 2D à partir d'un problème variationnel consistant à chercher le minimum de l'enstrophie totale tout en conservant l'énergie cinétique et la circulation dans le domaine de calcul. Cette approche est liée à la théorie MRS ([7, 9]). Nous obtenons ainsi les états d'équilibre les plus probables en fonction des paramètres de contrôle et de la géométrie du problème. Nous avons résolu numériquement ce problème et obtenu les ~~différents~~ différentes courbes caloriques et les diagrammes de phase. Une bifurcation entre une solution à un tourbillon ("zonale") ou à deux tourbillons ("bloquée") a été identifiée, ce qui semble confirmer l'existence d'états meta-stables dans des écoulements autour d'un obstacle central.

Abstract :

Rod bundle flows inside nuclear cores of pressurized water reactors (PWR) are mainly aligned with the direction parallel to the rods. In the planes orthonormal to this direction, some secondary flows occur and play an important role in the thermal mixing characteristics. These flows exhibit spontaneous reorganisations that seem comparable to the phase transitions observed between meta-stable states of the Northern Hemisphere atmosphere (~~Corvellec~~ [5]). In order to put forward an explanation of this phenomenon, equilibrium states of the 2D Euler equations are computed from a variational problem consisting in minimizing the total enstrophy function (related to entropy) while conserving kinetic energy and circulation inside the domain. This method can be related to MRS theory ([7, 9]). We obtain the most probable equilibrium states depending on control parameters and geometry here restricted to the representative configuration of a ring-shaped domain. We have solved numerically this problem and obtained the different caloric curves and phase diagrams. A bifurcation between 1-eddy ('zonal') and 2-eddy ('blocked') solutions has been identified, confirming the existence of meta-stable states in flows containing a central obstacle.

Keywords :

Rod bundle flows, Statistical fluid mechanics, Euler 2D, Bifurcation, Meta-stable states

1 Introduction

The prediction of the thermal mixing in Pressurized Water Reactor (PWR) fuel assemblies is of major importance in nuclear reactor safety assessment aimed at evaluating the thermal conditions during the reactor normal operation. The core of a PWR is constructed from an array of nuclear fuel rods positioned by support grids at specific axial distances. Mixing vanes are placed on the top edges of the grids to enhance the heat transfer in subchannels. The water flows mainly in the direction parallel to the rods. Due to the mixing vanes, some secondary flows occur in planes orthonormal to the axial direction. Forced convection is used to transport the thermal energy from the surfaces of the rods to the bulk of the fluid. The flow field in the fuel assembly is very complex due to the geometry of the subchannels and the high axial component of the velocity field relative to the secondary flows. Starting from the mixing grid, both the cross flow imposed by the vanes and the turbulence intensity develop axially. Turbulence is very strong just downstream of the mixing vanes, and it decays as the flow travels downstream of these vanes. The boiling point margin is reduced with distance from the mixing vane due to the reduction of both the turbulence level and the cross flow velocity. It is then crucial to understand and predict the flow field behaviour in the far wake of the mixing grids.
To analyze such a developing flow field, an experiment performed in the AGATE facility (see [6]) has been simulated with the Trio_U[1] code [1]. The AGATE experiments have originally been designed to characterize different types of mixing grids. The test section consists of a 5×5 tube bundle and a mixing grid, which are placed within a metallic channel of a quadratic cross section. The specific point we are interested in is that the experiment shows a reorganization of the cross flow not visible numerically. As shown on Figure 1, the transverse flow displays large-scale structures, which right after the mixing grids are aligned with a diagonal of the square box with a 45° angle. Surprisingly, this transverse flow was observed to spontaneously rearrange itself further downstream, apparently along the other diagonal of the square box with a 135° angle. The simulations fail in reproducing this flow field reorganization experimentally observed from a certain distance downstream far from the grid. This rearrangement has important consequences on the rod bundle cooling efficiency. However, no explanation of this phenomenon was advanced by previous experimental and numerical studies. This is the motivation of the present work.

A remarkable feature of the transverse flow is the relative decorrelation between the velocity component parallel to the rod axes and its components in the transverse plane, at least in the bulk of the flow (out of the boundary layers). This feature allows us to assume that the 3D flow behaves in a first approximation as a "transported 2D flow". Following this assumption, the flow in the transverse plane (hereafter designated as the transverse flow) abides by 2D fluid dynamics. Furthermore, because of the high value of the considered Reynolds number ($Re \simeq 10^5$) and considering the fact that we exclude the boundary layer, we neglect the viscosity and place our study in the theoretical frame of the 2D Euler equations.
The large-scale flow patterns shown in figure 1 exist during time scales much larger than the turbulence time scales, and they seem to drastically shift between one another. These characteristics are reminiscent of meta-stable phenomena typically observed for example in 2D geophysical flows [5] and studied by statistical mechanics tools. Such 2D geophysical flows include the Jupiter Red Spot [**?**], the Kuroshio path and the Gulf Stream [10]. The aim of the present work is to make an analogy between the reorganisation of the flow field observed in the AGATE facility and phase transitions between dif-

[1]The Trio_U code has recently been renamed TrioCFD [1].

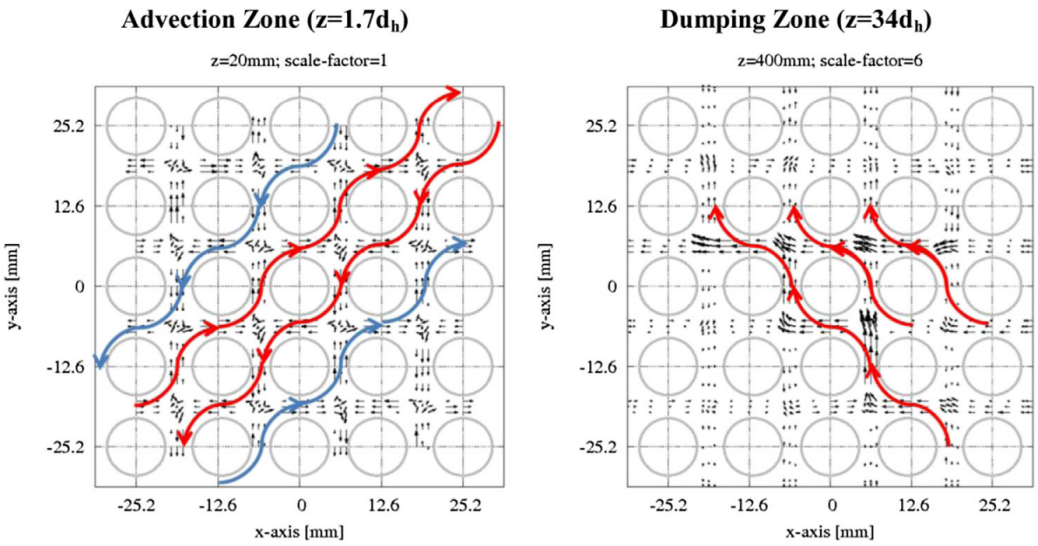

FIG. 1 – Large coherent flow patterns appearing in the AGATE experiments, right after the mixing grid (left) and further downstream (right). From Bieder et al. [2]

ferent equilibrium states obtained through the sufficient condition of minimal enstrophy under specific constraints (i.e. through the Minimal-Enstrophy Principle, which can be related to other theories such as MRS by [7, 9]).

In Section 2, the theoretical framework of the study is presented. Section 3 details the numerical method used to compute solutions of this variational problem for given control parameters and in a non-trivial domain. Some solutions obtained for various geometrical domains are presented in section 4. Classical results are first obtained in order to show the validity of the numerical method. Calculations are then performed on a non-simply connected domain, which adds the constraint of the circulation around the central obstacle and induces new bifurcation possibilities.

2 Theoretical framework

We consider the two-dimensional vorticity equations (derived from the incompressible Euler equations) written as

$$\begin{cases} \dfrac{\partial \omega}{\partial t} + \mathbf{u} \cdot \nabla \omega = 0, \\ \\ \omega \mathbf{z} = \nabla \times \mathbf{u}, \end{cases} \tag{1}$$

where ω is the vorticity, $\mathbf{u}$ the velocity field, and $\mathbf{z}$ a unit vector normal to the flow. Let ψ be the stream function defined as

$$-\Delta \psi = \omega. \tag{2}$$

The 2D Euler equations admit an infinite number of steady states of the form $\omega = f(\psi)$ where f is an arbitrary function. These solutions are obtained by solving

$$\begin{cases} -\Delta \psi = f(\psi) = \omega \\ \psi = a \in \mathbb{R}, \text{ on the domain boundary.} \end{cases} \tag{3}$$

The idea is to determine, among the infinite number of steady states, those ones that are stable, according to the equilibrium statistical theory developed in [7, 9] and [8].
The exact vorticity field can be decomposed as a sum of a local average (coarse-grained) vorticity $\overline{\omega}$ and a fluctuating term containing the very small scales that cannot be numerically computed. Ultimately, the vorticity level distribution will be given by CFD simulations. The problem is solved in the variable ψ, then the solutions (named *macroscopic solutions*), denoted by $\overline{\psi}$ verify $-\Delta\overline{\psi} = \overline{\omega}$ and contain only large-scale fluctuations.

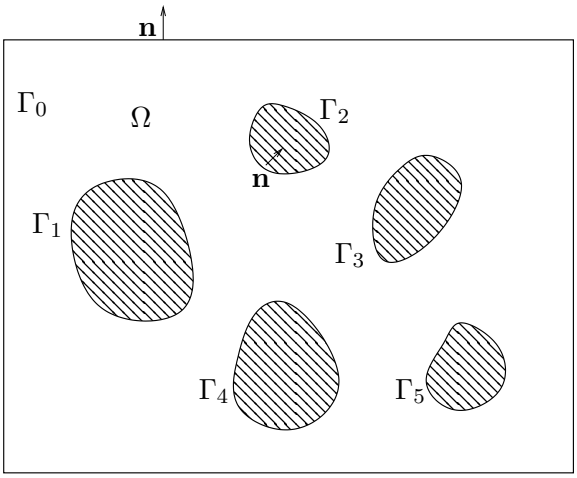

FIG. 2 – Schematic representation of the domain for $Q = 5$.

Let Ω be a bounded polygon of $\mathbb{R}^2$, the boundary of which is denoted by Γ. We suppose that the domain has Q obstacles, $Q \geq 0$. Let Γ_0 denote the exterior boundary of Ω and let Γ_q with $q \in [1, Q]$ be the interior polygonal boundary of Ω, so that $\Gamma = \Gamma_0 \cup_{q\in[1,Q]} \Gamma_q$.

The solution ψ satisfies (to simplify the notation the $\bar{\cdot}$ is omitted)

$$\begin{cases} -\Delta\psi &= \omega, \quad \Omega \\ \psi &= a_q, \quad \Gamma_q,\ q \in [0, Q] \end{cases} \tag{4}$$

The non-penetration condition for the fluid at a boundary Γ imposes that $\mathbf{u}\cdot\mathbf{n} = \mathbf{0}$, with $\mathbf{n}$ a normalized vector normal to the boundary Γ. This leads to $\nabla\psi \cdot \mathbf{n}^{\perp} = \mathbf{0}$. Then, ψ must have a constant value on each piece of boundary Γ_q, which is generally set at the arbitrary value of zero. However, assuming that different pieces of boundary have the same value for ψ is a restriction on the ensemble of available values for the control parameters. Since several pieces of boundary are here considered in the problem definition (4), we only impose $a_0 = 0$.

The averaging operator $\langle\cdot\rangle$ on Ω is defined as

$$\langle X \rangle = \frac{\displaystyle\int_{\Omega} X \, d\mathbf{r}}{\displaystyle\int_{\Omega} 1 \, d\mathbf{r}}, \tag{5}$$

allowing the domain to have an area $\displaystyle\int_{\Omega} 1 \, d\mathbf{r} \neq 1$. $\displaystyle\int_{\Omega} 1 \, d\mathbf{r} = |\Omega|$ in the following.
We introduce the enstrophy, the circulation and the energy defined as functions of the variable ψ as

$$S[\psi] = \frac{1}{2}\langle \Delta\psi\Delta\psi \rangle, \quad C[\psi] = \langle \Delta\psi \rangle = \frac{\displaystyle\int_{\Gamma} \nabla\psi\cdot\mathbf{n} d\sigma}{|\Omega|}, \quad E[\psi] = \frac{1}{2}\langle \nabla\psi\nabla\psi \rangle. \tag{6}$$

The total circulation can be developed as $\mathcal{C} = \displaystyle\sum_{q=0}^{Q} \mathcal{C}_q = \sum_{q=0}^{Q} \oint_{\Gamma_q} \nabla\psi\cdot\mathbf{n} d\sigma$.

Following Naso [8], the most probable solution in the sense of the Minimum-Enstrophy-Principle

(MEP) is the solution of the variational problem :

$$\min_{\psi} \left\{ S[\psi] | E[\psi] = \overline{E}, \mathcal{C}[\psi] = \overline{\mathcal{C}}, \mathcal{C}_q[\psi] = \overline{\mathcal{C}_q}, q = 1, \ldots, Q \right\}, \tag{7}$$

Remark that no condition is imposed on Γ_0 since $\mathcal{C} = \mathcal{C}_0 + \sum_{q=1}^{Q} \mathcal{C}_q$.

To minimize enstrophy under the constraints of conserved energy E and circulation $\mathcal{C}$ and $\mathcal{C}_q$ ($q = 1, \ldots, Q$), we introduce the Lagrange parameters β, α and α_q ($q = 1, \ldots, Q$) and the functional

$$\begin{aligned} J(\psi) = S(\psi) - \beta \left(\frac{1}{2} \langle \nabla\psi \cdot \nabla\psi \rangle - \overline{E} \right) - \alpha \left(\langle \Delta\psi \rangle - \overline{\mathcal{C}} \right) \\ - \sum_{q=1}^{Q} \alpha_q \left(\frac{\oint_{\Gamma_q} \nabla\psi \cdot \mathbf{n} d\sigma}{|\Omega|} - \overline{\mathcal{C}}_q \right) \end{aligned} \tag{8}$$

In order to write the variational form for the optimization problem J we compute (with $\phi|_\Gamma = 0$)

$$\begin{aligned} J(\psi + \theta\phi) = J(\psi) - \theta \langle \Delta\psi \Delta\phi \rangle - \frac{1}{2}\theta^2 \langle \Delta\phi \Delta\phi \rangle \\ -\beta\theta \langle \nabla\psi \cdot \nabla\phi \rangle - \frac{1}{2}\beta\theta^2 \langle \nabla\phi \cdot \nabla\phi \rangle \\ +\alpha\theta \langle \Delta\phi \rangle - \theta \sum_{q=1}^{Q} \alpha_q \frac{\oint_{\Gamma_q} \nabla\phi \cdot \mathbf{n} d\sigma}{|\Omega|}. \end{aligned} \tag{9}$$

By imposing the constraint $\nabla\phi \cdot \mathbf{n} = 0$ on Γ we get the local problem satisfied by the solution ψ of the optimization problem

$$\Delta\psi = \beta\psi + \alpha = -\omega. \tag{10}$$

Taking the space integral of (10) :

$$\int_{\Omega} \Delta\psi \mathrm{d}\mathbf{r} - \beta \int_{\Omega} \psi \mathrm{d}\mathbf{r} = \alpha \int_{\Omega} 1 \mathrm{d}\mathbf{r}, \tag{11}$$

which considering the expression defined for the averaging operator leads to

$$\alpha = \langle \Delta\psi \rangle - \beta \langle \psi \rangle = \mathcal{C} - \beta \langle \psi \rangle. \tag{12}$$

Replacing α by its expression in (10) leads to the fundamental equation to be solved

$$-\Delta\psi + \beta\psi = \mathcal{C} + \beta \langle \psi \rangle. \tag{13}$$

3 Case of a domain with no obstacle ($Q = 0$)

Equation (13) is first solved in the simple case of homogeneous Dirichlet boundary conditions, as presented in [4] and [8]. This preliminary step will enable us to validate the numerical solver.

3.1 Resolution method

The fundamental equation to be solved here is

$$-\Delta\psi + \beta\psi = \mathcal{C} + \beta \langle\psi\rangle \tag{14}$$

with $\psi = 0$ on the boundary. Expression for the kinetic energy can be obtained using (6) and (13) :

$$E = \frac{1}{2}\langle\nabla\psi\nabla\psi\rangle = -\frac{1}{2}\langle\psi\Delta\psi\rangle = -\frac{1}{2}\beta\left(\langle\psi^2\rangle - \langle\psi\rangle^2\right) + \frac{1}{2}\mathcal{C}\langle\psi\rangle. \tag{15}$$

Decomposition of the Laplacian in an eigenbasis

Assuming in a first step that $\alpha = 0 \Leftrightarrow \mathcal{C} = -\beta\langle\psi\rangle$, equation (14) becomes

$$-\Delta\psi + \beta\psi = 0. \tag{16}$$

Equation (16) is a Laplacian problem ; let $(\beta_i, e_i)_{i=1..N}$ be an orthonormal eigenbasis of the Laplacian operator, with the eigenvectors $(e_i)_{i=1..N}$ verifying

$$\langle e_i \cdot e_j\rangle = \delta_{ij},\ e_{i|\Gamma} = 0. \tag{17}$$

with δ_{ij} the Kronecker symbol. Solutions of (16) exist when β is an eigenvalue β_i. The solutions $\psi = \psi_E e_i$ then are the eigenvectors e_i respectively associated with these eigenvalues normalized by a constant ψ_E. The normalization constant is obtained by injecting ψ into (15) knowing that $\mathcal{C}+\beta\langle\psi\rangle = 0$ by hypothesis :

$$E = -\frac{1}{2}\beta_i\psi_E^2\langle e_i^2\rangle \implies \psi_E = \sqrt{-\frac{2E}{\beta_i}}. \tag{18}$$

Injecting (18) into $\mathcal{C}^2 = \beta_i^2\langle\psi\rangle^2$ gives

$$\mathcal{C}^2 = -2E\beta_i\langle e_i\rangle^2. \tag{19}$$

Following [4], the parameters E and $\mathcal{C}$ are combined into the control parameter Λ^2 defined as

$$\Lambda^2 = \frac{\mathcal{C}^2}{2E}, \tag{20}$$

which allows for a simpler representation of the bifurcations presented thereafter.

The Λ parameter can immediately be used to group the parameters $(E, \mathcal{C})$ in (19) into

$$\Lambda^2 = -\beta_i\langle e_i\rangle^2. \tag{21}$$

In the case of zero-mean eigenvectors, $\langle e_i\rangle = 0 \implies \Lambda = 0$. Several such eigenvectors in the case of the empty bounded square domain are plotted on figure 3 and 4, on the line corresponding to $\Lambda = 0$.

The continuous branch

The case $\alpha = \mathcal{C} + \beta\langle\psi\rangle \neq 0$ is thereafter considered ; let ϕ be defined as

$$\phi = \frac{\psi}{\mathcal{C} + \beta\langle\psi\rangle}, \tag{22}$$

which allows to modify equation(14) into the differential equation

$$-\Delta\phi + \beta\phi = 1 \tag{23}$$

with $\phi = 0$ on the boundary. Assuming that $\beta \neq \beta_i$, the orthonormal eigenbasis $(e_i)_{i=1..N}$ is used to decompose ϕ as

$$\phi = \sum_i \frac{\langle e_i \rangle}{\beta - \beta_i} e_i. \tag{24}$$

Taking the average of equation (22) : $\langle\psi\rangle = \mathcal{C}\langle\phi\rangle/(1 - \beta\langle\phi\rangle$, we can express ψ as a function of ϕ as :

$$\psi = \frac{\mathcal{C}\phi}{1 - \beta\langle\phi\rangle}. \tag{25}$$

Replacing (25) into (15) to take into account the energy constraint, the "equation of state" $\Lambda = f(\beta)$ is obtained :

$$(1 - \beta\langle\phi\rangle)^2 = \Lambda^2(\langle\phi\rangle - \beta\langle\phi^2\rangle). \tag{26}$$

The eigenbasis $(e_i)_{i=1..N}$ and the set of eigenvalues $(\beta_i)_{i=1..N}$ being set by the geometry, fixing an arbitrary value for β allows the calculation of Λ with (26). A "continuous solution" ψ_{cont} associated to Λ^2_{cont} can therefore be calculated for each value of β. The $\Lambda^2_{cont} = f(\beta)$ plot then available is refered to as the "continuous branch".

For eigenvectors such as $\langle e_i \rangle \neq 0$, let us consider the case of $\beta \to \beta_i$:

$$\phi \underset{\beta\to\beta_i}{\sim} \frac{\langle e_i \rangle}{\beta - \beta_i} e_i \implies \Lambda^2 \underset{\beta\to\beta_i}{\to} -\beta_i \langle e_i \rangle^2 \tag{27}$$

The value of Λ obtained for the eigenvectors of non-zero mean value in (21) is recovered in the "continuous" branch, i.e. the pure eigenvector solutions of non-zero mean value are contained in the "continuous" branch.

The mixed solutions

More solutions of the fundamental equation (14) can be obtained by combining a zero-mean eigenvector e_i with the continuous solution for $\beta = \beta_i$, creating "mixed solutions". They are defined as

$$\phi_{mix}(\beta_i) = \phi_{cont}(\beta_i) + \chi_i e_i = \sum_{j\neq i} \frac{\langle e_j \rangle}{\beta_i - \beta_j} e_j + \chi_i e_i, \tag{28}$$

with i such that $\langle e_i \rangle = 0$ and $\chi_i \in \mathbb{R}$. This leads through (25) to

$$\psi_{mix}(\beta_i) = \frac{\mathcal{C}\phi_{mix}(\beta_i)}{1 - \beta_i \langle \phi_{mix}(\beta_i) \rangle} = \frac{\mathcal{C}\phi_{mix}(\beta_i)}{1 - \beta_i \langle \phi_{cont}(\beta_i) \rangle} = \psi_{cont}(\beta_i) + \frac{\mathcal{C}\chi_i e_i}{1 - \beta_i \langle \phi_{cont}(\beta_i) \rangle}. \tag{29}$$

Solutions $\psi_{mix}(\beta_i)$ verify equation (13) since $\psi_{cont}(\beta_i)$ is already a solution, the fundamental equation is linear, and $\langle e_i \rangle$ is a zero-mean eigenvector.

The mixed solutions include the continuous branch for $\beta = \beta_i$ as a limit case for $\chi_i = 0$; it is there straightforward that $\psi_{mix}(\beta_i) \underset{\chi_i=0}{=} \psi_{cont}(\beta_i)$ and $\Lambda_{mix}(\beta_i) \underset{\chi_i=0}{=} \Lambda_{cont}(\beta_i)$. The zero-mean eigenvector

e_i is recovered in the limit case $\chi_i \to \infty$, as $\phi_{mix} \underset{\chi_i \to \infty}{\sim} \chi_i e_i$ and $\Lambda_{mix} \underset{\chi_i \to \infty}{\to} 0$.

For $\Lambda_{mix}(\beta_i) \neq 0, < \Lambda_{cont}(\beta_i)$, the value of χ_i is obtained by using the energy constraint through the injection of (28) into (15).

These "mixed solutions" thus form a continuous transition between
– the zero-mean eigenvectors verifying $\langle e_i \rangle = 0$ for $\Lambda = 0$ when $\chi_i \to \infty$.
– the continuous solution for $\Lambda_{mix}(\beta_i) = \Lambda_{cont}(\beta_i)$ when $\chi_i = 0$
This completes the problem resolution for the case without obstacle.

3.2 Validation of the method without obstacle

The resolution method explained in section 3 is used as a first step in order to recover classical results in the case of a square domain without any obstacles.

Combining the "continuous branch" and the mixed solutions allows to group all possible solutions ψ into the phase diagram plot. The phase diagram obtained for an empty square domain is shown on figure 3. ~~It is very similar to the corresponding plot~~ As expected, the results obtained by Chavanis [4] (shown on figure 4) for an identical problem are recovered.

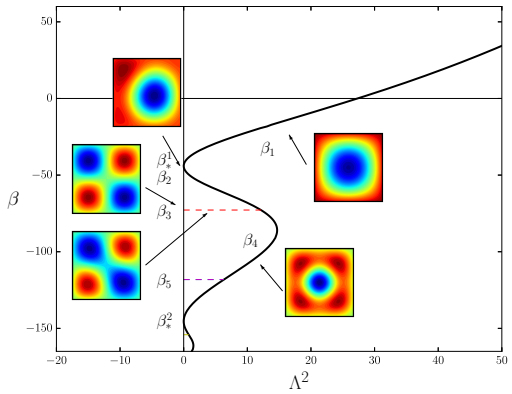

FIG. 3 – Phase diagram obtained for a bounded square box, with several significant solutions shown.

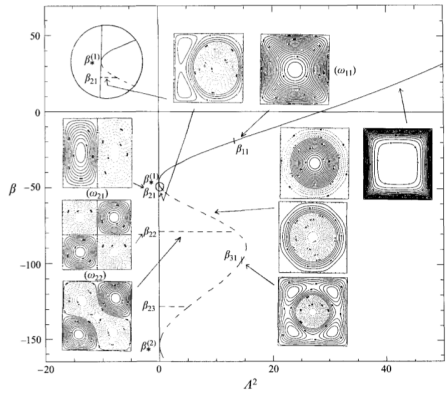

FIG. 4 – Phase diagram presented by Chavanis [4] for a bounded square domain.

On both of these plots, the continuous branch is shown with a thick black line, while the zero-mean eigenvectors appear on the $\Lambda = 0$ vertical line ($\beta_2, \beta_3, \beta_5$). Eigenvectors with a non-zero mean value are contained in the continuous branch (β_1, β_4). The mixed solutions are shown as horizontal, dashed lines between the continuous branch and the $\Lambda^2 = 0$ vertical line.

Search of the most probable solution

The ensemble of solutions shown in a phase diagram allows to look for the most probable solution ψ for any given Λ.

It can be shown (see [3],[4]) that the enstrophy is a strictly decreasing function of the Lagrange parameter β. Consequently, among the infinite set of available solutions for a given Λ, the most probable one is this statistical theory is the one corresponding to the greatest value of β.

In the particular case of the empty square domain as shown on figures 3 and 4, the most probable solution is the continuous one for any given Λ. Indeed the first mixed solution available at $\beta = \beta_2$ is

unreachable by the system even at small values of Λ because $\beta_2 < \beta_*^1$, with β_*^1 the highest β allowing the continuous solution to reach $\Lambda_{cont} = 0$.

As shown by [4] and [8], this arrangement of the different solution categories is very dependent on the geometry ; a rectangular domain induces quite different mechanisms. Indeed, the first zero-mean eigenvalue β_2 is then higher than β_*^1 for a rectangle of aspect ratio $\tau > 1.12$, which creates an interval of control parameters where the dipole (mixed solution based on the first pair of zero-mean eigenvalues) is more probable than the monopole (the continuous branch). A bifurcation is then observable between the two behaviours at a critical point Λ_{bif}^2.

In order to consider geometries more representative of the transverse flow in the AGATE facility, the following calculations are performed on non-simply connected domains, i.e. with a central obstacle. It is shown that such geometries induce bifurcations similar to those observed in rectangular domains between dipole and monopole states.

The case with obstacle ($Q > 1$) is described in the following section.

4 Complete case : domain with obstacle

4.1 Problem resolution

In that case, we are faced with the resolution of a Laplacian problem with non homogeneous Dirichlet boundary conditions. A variable transformation is used by introducing a function ψ_Γ which satisfies

$$\left\{ \psi_\Gamma = a_q, \quad \Gamma_q,\ q \in [0, Q] \right. \tag{30}$$

A new function Ψ is defined as $\psi - \psi_\Gamma$. Ψ is a solution of the local problem

$$-\Delta\Psi + \beta\Psi = \Delta\psi_\Gamma - \beta\psi_\Gamma + \mathcal{C} + \beta\left(\langle\Psi\rangle + \langle\psi_\Gamma\rangle\right). \tag{31}$$

As Ψ satisfies the homogeneous Dirichlet boundary conditions, it can be decomposed on the eigenbasis (β_j, e_j) of the Laplacian operator, as was done for the previous resolution in the case of homogeneous Dirichlet boundary conditions.

The solution ψ and its Laplacian $\Delta\psi$ are decomposed into :

$$\psi = \sum_{j=1}^{N} b_j e_j + \psi_\Gamma, \qquad \Delta\psi = \sum_{j=1}^{N} b_j \beta_j e_j + \Delta\psi_\Gamma \tag{32}$$

$$\text{with } e_j = 0 \text{ on } \Gamma_0 \text{ and } \Gamma_q,\ q \in [1, Q] \text{ and } \psi_\Gamma = a_q \text{ on } \Gamma_q,\ q \in [1, Q].$$

Injecting (32) into (13) allows to compute the coefficients b_j depending on the circulation $\mathcal{C}$, the Lagrange multiplier β and the constant function Ψ_R, and to express in the eigenbase $(e_j)_{j=1..N}$ the "continuous" solution ψ_{cont} :

$$\psi_{cont.}(\mathcal{C}, \beta, \psi_\Gamma) = \sum_{j=1}^{N} b_j(\mathcal{C}, \beta, \psi_\Gamma) e_j + \psi_\Gamma. \tag{33}$$

"Mixed" solutions ψ_{mix} can also be linearly computed as

$$\psi_{mix}(\mathcal{C}, \beta, \psi_\Gamma) = \psi_{cont}(\mathcal{C}, \beta, \psi_\Gamma) + x e_i,\ \forall x \in \mathbf{R} \tag{34}$$

with e_i an eigenvector such as $\langle e_i \rangle = 0$.

4.2 Results on non-simply connected domain

The resolution described in 4.1 was applied to more complex geometries presenting multiple pieces of boundary, in particular with a central obstacle in the domain, though still with homogeneous Dirichlet boundary conditions. The theoretical framework remains broadly the same when an obstacle is present ; the phase diagram obtained for both an annular domain and a square domain with a central obstacle are shown in figures 7 and 8. It can be immediately observed in these diagrams that a bifurcation occurs between 1- and 2-eddies states for a particular value of Λ^2_{bif}, as it was observed in the case of a rectangular domain. The 1- and 2-eddies states are respectively the continuous and mixed solutions.

These ~~two states observed in the case of the annular domain are coherent with the experimental findings of~~ findings can be compared to those obtained in the 2D-rotating tank experiment by Tian et al. [11]~~, who encountered in a 2D-rotating tank experiment two large-scale flow configurations, labeled as~~ . Depending on the forcing (through fluid influx/outflux and rotation of the tank), a bifurcation between two flow patterns was exhibited therein, as shown in figure 5 :

– a "zonal" ~~and~~ flow pattern featuring a dominant eddy around the central obstacle,
– a "blocked" ~~, as shown in figure 5.~~ flow pattern featuring a weaker central eddy with larger counter-rotating eddies.

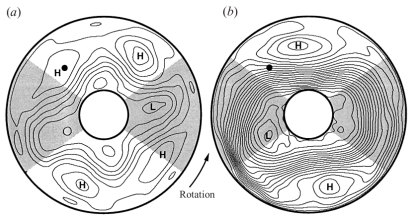

FIG. 5 – "Blocked" (a) and "zonal" (b) flow patterns observed by Tian [11] (Figure 2).

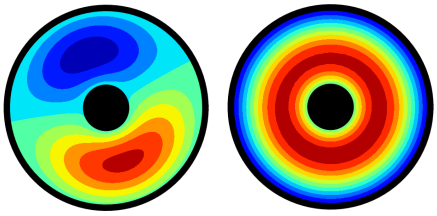

FIG. 6 – "Mixed" (left) and "continuous" (right) minimal-enstrophy solutions obtained.

~~A qualitative agreement between~~ Both in these experiments and ~~our results seems to be achieved, both in the fact that the 2D turbulent flow can exist in two distinct states, and in the mechanics of these states : a~~ in our results, a single phase transition is obtained. Qualitative similarities can also be found respectively between the shape of "zonal" ~~flow comprised of a dominant eddy around the obstacle a~~ flows and of the continuous solutions, and between the shape of "blocked" ~~flow with diminished importance of the main eddy but more significant secondary eddies on each side of the obstacle.~~ flows and of the mixed solutions. Although this comparison is drawn for precise values of the external parameters, it gives us confidence in the method used for non-simply connected domains.

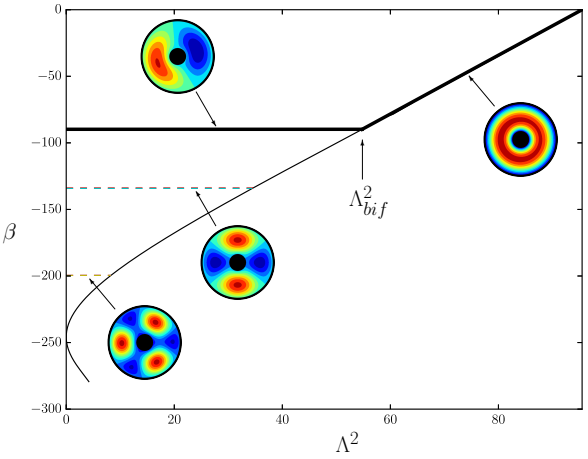

FIG. 7 – Phase diagram showing the "continuous" solution (thin black line), the "mixed" solutions (dashed horizontal lines) and the most probable solution (thick black line) in the cas of an annular domain, for $a_1 = 0$. The Λ^2 value corresponding to the bifurcation is denoted as Λ^2_{bif}.

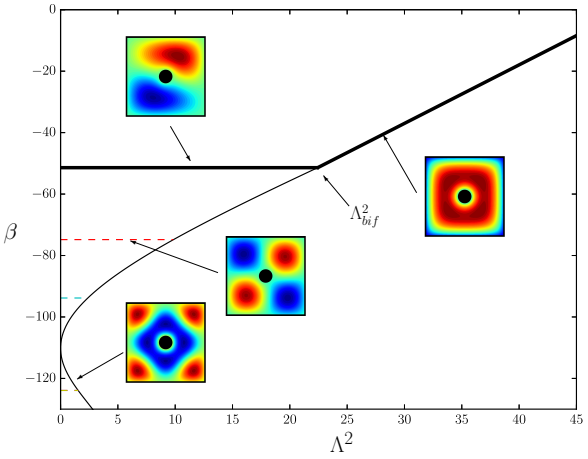

FIG. 8 – Phase diagram showing the "continuous" solution (thin black line), the "mixed" solutions (dashed horizontal lines) and the most probable solution (thick black line) in the case of a square with a central obstacle, for $a_1 = 0$. The Λ^2 value corresponding to the bifurcation is denoted as Λ^2_{bif}.

4.3 Non-homogeneous boundary conditions

These results obtained with $a_q = 0,\ q \in [1, Q]$ can be completed by varying a_q and computing the circulation around the central obstacle $\mathcal{C}_{obstacle}$. This allows to observe the fluctuation of the bifurcation parameter Λ^2_{bif}. The resulting plot is shown as the bifurcation diagram in figure 9 in the case of an annular geometry. It is there shown that existence zones for the two states (1-eddy or "zonal, and 2-eddies or "blocked") were found in the parameter space $(\Lambda^2, \mathcal{C}_{obstacle})$. The bifurcation line $\mathcal{C}_{obstacle} = f(\Lambda^2)$ is also shown as a thick black line.

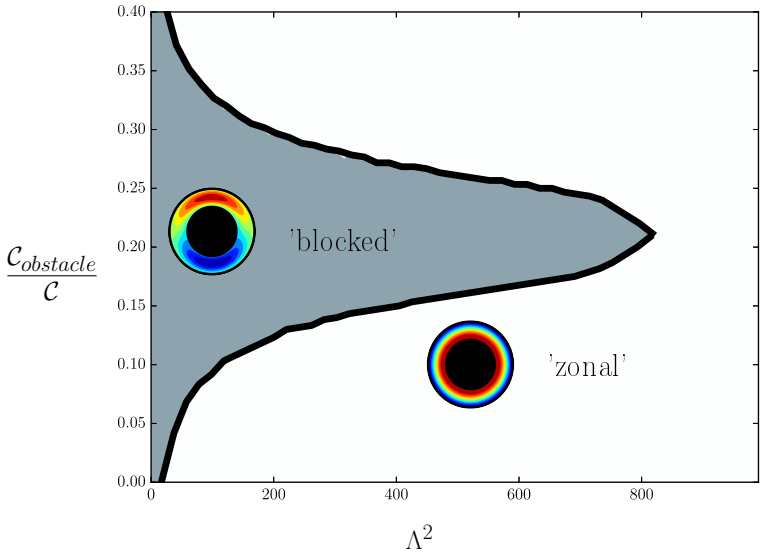

FIG. 9 – Bifurcation diagram showing the domination zones of the "mixed" ("blocked") and "continuous" ("zonal") solutions in parameter space, in the case of the annular domain. It was obtained by scanning E and $\mathcal{C}_{obstacle}$ values while keeping $\mathcal{C}$ constant.

5 Perspectives/conclusion

In the theoretical framework of statistical fluid mechanics in two-dimensions presented by [8], a numerical approach is designed and implemented to solve the variational problem (7) of minimal-enstrophy solutions under the constraints of E, $\mathcal{C}$ and $\mathcal{C}_q,\ q \in [1, Q]$ conservation. The lowest-enstrophy solution obtained allows to find the most probable flow pattern in both an annular domain and a square domain with a central obstacle.

Two particular regimes are identified ("mixed" and "continuous"), which are coherent with the "blocked" and "zonal" flows observed in the fast-rotating tank experiment by Tian [11]. The bifurcation between these regimes occurs for a particular value Λ^2_{bif}, which depends on the geometry and on the values chosen for the constraints (see Figure 9).

The existence of such multiple meta-stable states and the possibility that bifurcations happen between them for 2D flows around central obstacles is an important result for the comprehension of the experimental observations from the AGATE facility. Indeed, it seems likely that the behaviour that was here put into light for simple geometries exists in geometries including more obstacles as well.

Future work will consist in CFD calculations attempting to observe the simulated flow stabilizing onto the predicted minimal-enstrophy solutions, and ~~extension to~~ exploration of several multiple-obstacles cases in a parameter space limited to physically-relevant configurations.

Références

[1] TrioCFD : http ://www-trio-u.cea.fr/.

[2] Ulrich Bieder, François Falk, and Gauthier Fauchet. LES analysis of the flow in a simplified PWR assembly with mixing grid. *Prog. Nucl. Energy*, 75 :15–24, 2014.

[3] P. H. Chavanis. Dynamical and thermodynamical stability of two-dimensional flows : Variational principles and relaxation equations. *Eur. Phys. J. B*, 70(1) :73–105, 2009.

[4] P. H. Chavanis and J. Sommeria. Classification of self-organized vortices in two-dimensional turbulence : the case of a bounded domain. *J. Fluid Mech.*, 314 :267–297, 1996.

[5] Marianne Corvellec. *Phase transitions in two-dimensional and geophysical turbulence*. PhD thesis, 2012.

[6] F. Falk and A. Memponteil. Détermination d'un champ de vitesses 3D en géométrie complexe par vélocimétrie laser 2 dimensions. *Congrès Francoph. vélocimétrie laser*, pages H1.1–H1.6.

[7] Jonathan Miller. Statistical mechanics of Euler equations in two dimensions. *Phys. Rev. Lett.*, 65(17) :2137–2140, 1990.

[8] A. Naso, P. H. Chavanis, and B. Dubrulle. Statistical mechanics of two-dimensional Euler flows and minimum enstrophy states. *Eur. Phys. J. B*, 77(2) :187–212, 2010.

[9] Raoul Robert and Joel Sommeria. Statistical equilibrium states for two-dimensional flows. *J. Fluid Mech.*, 229 :291–310, 1991.

[10] Maurice J. SCHMEITS and Henk A. DIJKSTRA. Bimodal behavior of the Kuroshio and the Gulf Stream. *J. Phys. Oceanogr.*, 31(12) :3435–3456, 2001.

[11] Yudong Tian, Eric R Weeks, Kayo Ide, J S Urbach, Charles N Baroud, Michael Ghil, and Harry L Swinney. Experimental and numerical studies of an eastward jet over topography. *J. Fluid Mech.*, 438 :129–157, 2001.